

Tutorial

Olaf Stenzel* and Angus Macleod*

Metal-dielectric composite optical coatings: underlying physics, main models, characterization, design and application aspects

Abstract: Metal island films are a matter of research in different branches of applied physics and technology. One possible future application field is their use as a substantial part of optical interference coatings, forming metal-dielectric composite multilayer coatings. This tutorial provides background on optical specifics of metal island films and ideas how these specifics could be exploited in coating technology. Consideration is given to effective optical constants of copper and silver island films, characterization methods and design strategies pursuing neutral density filters, asymmetric beamsplitters and decorative coating specifications.

Keywords: coating design; metal island films; optical constants.

*Corresponding authors: Olaf Stenzel and Angus Macleod, Fraunhofer-Institut fuer Angewandte Optik und Feinmechanik IOF, Optical Coatings Department, Albert-Einstein-Str. 7, 07745 Jena, Germany; and Thin Film Center Inc., 2745 E Via Rotunda, Tucson, AZ 85716-5227, USA, e-mail: olaf.stenzel@iof.fraunhofer.de; angus@thinfilmcenter.com

1 Introduction

Metal island films represent a particular case of nanostructured cluster material [1]. They are built as a (nearly) planar arrangement of individual noble metal particles (in the following, we will call them ‘clusters’ or ‘islands’) with characteristic sizes usually ranging from a few to a few tens of nanometers. They may effectively absorb light due to the excitation of surface plasmons as well as characteristic interband transitions, and are therefore a natural choice as building blocks for spectrally selective absorbers.

For practical use of such island films in applied optics, and particular in coating technology, it is absolutely

necessary to have theoretical tools to hand, which allow reliable simulation of their optical properties. So far, diverse methods have been developed to quantify the specific effects of cluster size, shape, orientation, arrangement and environment of the individual islands on the optical properties of an island film. The basic theory was developed by Gustav Mie [2, 3] more than 100 years ago. In the quasistatic approximation, when the size of an individual cluster (or island) is much smaller than the wavelength of the light, simpler equations apply for the response of a single island, and particularly effects caused by deviations from a spherical island shape can be described in terms of ‘depolarization factors’ [4–6]. Yamaguchi et al. also discussed the influence of a non-symmetric dielectric environment of the clusters [7]. In the work of Gerardy and Ausloos [8], a so-called generalized Mie theory was developed with the purpose to calculate absorption and scattering losses of aggregates of spherical clusters [9], taking the electrodynamic interaction between the single clusters into account. Lebedev et al. [10, 11] extended that description to the practically relevant case of an absorbing cluster environment.

By contrast, it appears troublesome to combine the mentioned theoretical approaches with the standard theory of interference coatings in order to get easy-to-handle design and characterization tools. Once Mie’s theory operates with spherical waves, there is no *a priori* guaranteed compatibility to optical coating theory, which is based on the assumption of planar incident waves. Fortunately, in many practically relevant situations, the direct application of Mie’s theory or their derivations is not necessary. Owing to the small size of the metal islands and their small inter-island distances, the description of the optical properties of island films can often be performed within the limits of a homogeneous layer model [12] introducing ‘effective optical constants’ of the metal island film (i.e., the mixture of the islands and the embedding dielectric) [13]. Then these island films become accessible to typical thin film design and characterization software. However, the dispersion of these effective optical constants can look

unfamiliar to optical coating experts, so that some rather specialized optimization routines typically applied in thin film design may fail to converge. The purpose of this tutorial is to discuss the typical dispersion behavior of the effective optical constants of such metal island films, as well as to demonstrate examples on characterization and design of optical coatings with incorporated metal island films.

2 Effective optical constants of metal island films

The linear optical properties of a non-magnetic, optically homogeneous and isotropic material are completely determined by the behavior of the frequency-dependent complex index of refraction:

$$\hat{n}(\omega) = n(\omega) + ik(\omega) \quad (1)$$

Its real part n is nothing else than the ordinary refractive index, while its imaginary part k is called the extinction coefficient of the medium. n and k form the pair of linear optical constants of a non-magnetic medium; their dependence on the frequency is called ‘dispersion’.

By contrast, the complex index of refraction is connected to the complex dielectric function ε of the material through the relationship:

$$\hat{n}(\omega) = \sqrt{\varepsilon(\omega)} \quad (2)$$

Knowledge of the dielectric function is of utmost importance for understanding effects of the light-matter interaction, because it is connected to the ability of the medium to form an induced dipole polarization once it is

excited by the electric field of a light wave. Therefore, all dispersion models in solid state physics are originally formulated in terms of the dielectric function. Then, by using Eqs. (1) and (2), the refractive index and extinction coefficient may be calculated in a straightforward manner.

Similar to other branches of physics, in optical coating theory it makes sense to divide the materials available into two principal classes: electrical conductors and insulators. In insulators, all electrical charges have to be imagined to be somehow bound to some well-defined position in the solid (i.e., they are not allowed to move far away for their ‘regular’ positions). Nevertheless, small elongations from that position are allowed. By contrast, conductors are characterized by a certain amount of free charge carriers (in our case electrons), which can freely move through the material and thus contribute to a dc electrical conductivity. That division is rather useful in practice. It turns out, that in classical physics, the optical response of both free and bound charge carriers can be described by rather compact mathematical expressions, namely the so-called Lorentzian oscillator model for bound charge carriers, and the Drude model for free carriers. The corresponding equations (and their derivation) can be found in textbooks [3, 13]; they are given for completeness in Figure 1 together with a sketch of the typical dependence of the optical constants described by the relevant model on the frequency of the incoming light.

When looking at Figure 1 (left), the most striking feature in the optical response of a system with bound charge carriers is ‘resonance behavior’ in the extinction coefficient of a dielectric, when the frequency of the incident light comes close to the eigenfrequency ω_0 of the dielectric. In this case, strong dipole vibrations of the charge carriers around their equilibrium positions are observed, while the required

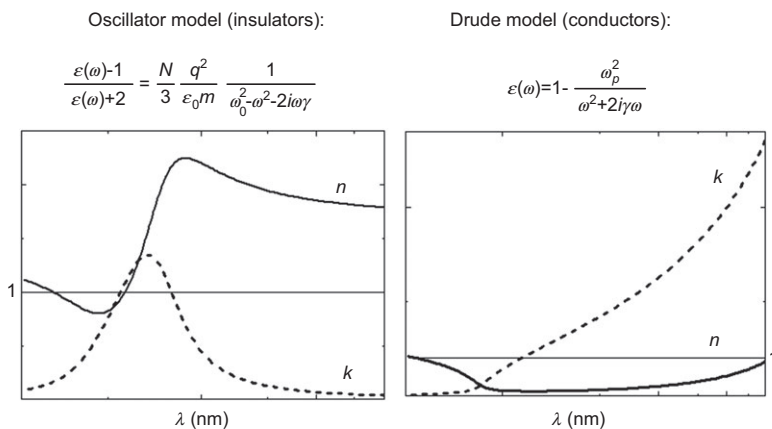


Figure 1 Principal dispersion behavior of the optical constants described by the oscillator model (left) and Drude model (right). N is the concentration of the bound charge carriers, m is their mass, and q their charge. ω_p is the plasma frequency of the free charge carriers, and γ is the damping parameter. ε_0 is the permittivity of free space. The wavelength scale is reciprocally stretched for preserving symmetry of the dispersion curves.

energy is taken from the incident light field. Therefore, the latter is damped in intensity when propagating through the medium, which is registered by a spectrophotometer as an absorption line. Apart from the resonance, extinction might be negligible, so that no light damping is observed and the dielectric appears transparent with a refractive index which is almost real. When designing a dielectric interference stack, we therefore usually make use of dielectrics with eigenfrequencies that are well outside the spectral region where the stack is specified.

This is in strong contrast to the optical behavior described by the Drude function. In this case, the real part of the refractive index may be significantly smaller than the value one in broad spectral regions, while the extinction coefficient is remarkably higher. Substituting these optical constants into the Fresnel equations for interface reflection, it can easily be shown that they will result in high reflection at the air-material interface, a behavior that is typically observed for metals which are good electrical conductors. It thus turns out that the typical optical appearance of metal surfaces is dominated by the response of the free electrons over large spectral regions.

However, the situation may change when the motion of the free electrons inside a metal is confined to a small (nanometer-sized) metal cluster, a situation which may be observed in composite materials, for example, the so-called metal island films. Such a situation is shown in Figure 2. In Figure 2, small copper clusters (or islands) are visualized by means of an electron microscope. The dark spots represent the copper islands, whereas the bright areas show the matrix formed in this case by an alumina film. Once alumina is an insulator, the ‘free’ copper electrons can no longer move freely through the medium, because the electrically conducting islands are well segregated from each other by a dielectric. In some regard,

the previously ‘free’ electrons now appear bound to the islands. When being optically excited, they may perform collective oscillations, thus causing strong surface charges which form a huge oscillating electric dipole moment. The oscillation of the electron cloud on the background of the rather immobilized cores is often called a localized surface plasmon. Once the electrons have a finite mass and feel a restoring force which does not permit them to leave the island, their movement is expected to show a resonance behavior, so that the optical behavior of a metal island film is rather expected to result in optical constants such as that shown on the left in Figure 1 than in the typical behavior of bulk metals as shown on the right of Figure 1.

When looking at Figure 2 it also becomes clear that for the presented example, both island sizes and typical inter-island distances are well below the wavelength of visible light. This makes it possible to tackle the island film as an optically homogeneous material. Then, its macroscopic optical behavior may be described by a pair of optical constants, which we will call ‘effective optical constants’, because they are defined by the optical constants of its constituents and the way in which they are mixed. The simplest analytical expression for the effective optical constants of a mixture like that shown in Figure 2 is given by the so-called Maxwell Garnett model (indicated in Figure 2) [1].

As promised previously, it is formulated in terms of the dielectric functions of the host material (alumina in our case), the guest material (copper in our case), as well as the volume filling factor of the guest material p_{guest} and some geometry-dependent value L called the depolarization factor. When all these values are accurately known, the dielectric behavior of the mixture (and consequently its effective optical constants n_{eff} and k_{eff}) may, in principle, be predicted. Hereby, we make use of the definition:

$$\hat{n}_{\text{eff}}(\omega) = n_{\text{eff}}(\omega) + ik_{\text{eff}}(\omega) \equiv \sqrt{\epsilon_{\text{mixture}}(\omega)} \quad (3)$$

It is intuitively understandable that the effective optical constants of a mixture ‘must’ somehow depend on those of its constituents as well as their relative weight as defined by the filling factor. Once this dependence is rather transparent, let us look instead at the depolarization factor L in more detail. What is its function in the model?

Let us imagine a metal cluster of spherical shape (Figure 3, left). Because of its high symmetry, its optical response should not depend on the orientation of the electric field vector. Such an island would appear completely isotropic with respect to its optical behavior.

The situation changes when the cluster is of ellipsoidal shape (Figure 3, right). Let us, for example, assume that the cluster is strongly elongated along the x -axis. It should be

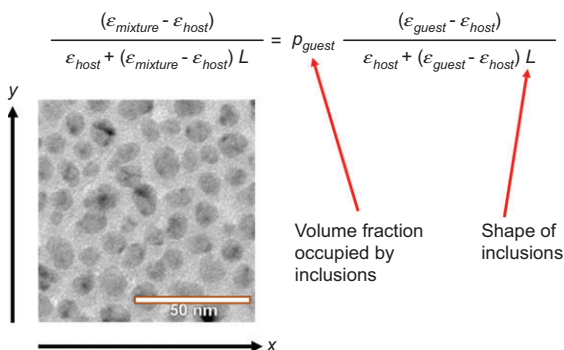


Figure 2 TEM image of a copper island film and Maxwell Garnett model for calculating the dielectric function of the mixture. The islands are arranged in the x - y plane, we will refer to it further as the ‘island film plane’.

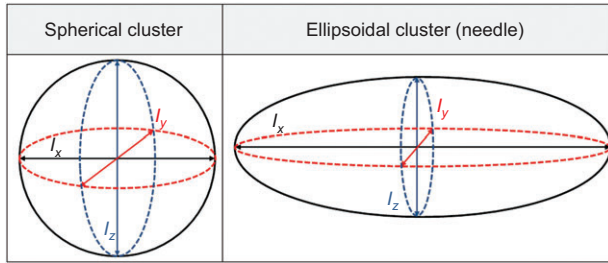


Figure 3 The definition of l_x , l_y and l_z .

intuitively clear that the response of the cluster to an electric field parallel to the x -axis will strongly differ from that caused by a field directed along the y -axis or z -axis. Indeed, once the field is directed along the x -axis, the electrons accelerated by the field may move over much longer distances than in the other cases. Therefore, an x -component of the exciting field will cause a response closer to that of a bulk metal than other field polarizations, which ‘try to’ accelerate the electrons into directions where their motion is more strongly confined. As a consequence, the surface plasmon resonance frequencies mentioned before will be different for different polarizations, it is lowest for oscillations along the longest axis, and it is highest along the shortest axis. In terms of the Maxwell Garnett model, this effect can be considered as introducing different depolarization factors.

In principle, for any ellipsoid, the depolarization factor responsible for one of the main directions can be calculated according to:

$$L_j = \frac{l_x l_y l_z}{2} \int_0^\infty \frac{ds}{(s+l_j^2) \{(s+l_x^2)(s+l_y^2)(s+l_z^2)\}^{1/2}}, \quad (j=x, y, \text{ or } z). \quad (4)$$

For many practical cases, one can keep in mind that $L=1/3$ for a spherical cluster excited along any direction. Once the cluster is deformed, the depolarization factors will differ from that value, while the normalization rule will be strictly fulfilled.

$$L_x + L_y + L_z = 1 \quad (5)$$

As a rule of thumb, excitation parallel to a long axis will correspond to a low depolarization factor, and vice versa. For extreme special cases, the depolarization factors are summarized in Table 1.

To highlight the impact of the depolarization factors, in Figure 4 some modeled effective optical constants are shown, corresponding to a 50:50 mixture of copper islands in an alumina matrix. The calculations have been performed assuming depolarization factors of $L=0.333$ (spherical clusters, black curves), $L=0.6$ (moderately flat pancakes excited along their main symmetry axis), and $L=0.2$ (the same pancakes excited normal to their main

Shape of inclusion	E parallel to the symmetry axis	E perpendicular to the symmetry axis
Sphere	$1/3$	
Infinitely long needle	0	$1/2$
Infinitely broad pancake	1	0

Table 1 Depolarization factors L .

E denotes the vector of the electric field strength.

symmetry axis), and assuming $p_{\text{guest}}=0.5$ in every calculation. All curves show the expected resonance behavior, while the choice of L has a dramatic effect on the resonance position. For comparison, in Figure 5 the assumed optical constants of the constituents are sketched. Note that the effective optical constants of the 50:50 mixtures can by no means be tackled as some average of the optical constants of alumina and copper.

As it follows from the calculations shown in Figure 4, a single ellipsoidal cluster will therefore necessarily appear optically anisotropic. However, as long as ellipsoidal clusters are randomly distributed with respect to their orientation in the volume of a sample, the mixture as a whole may still appear optically isotropic.

Although the real metal island film shown in Figure 2 represents a rather two-dimensional arrangement of copper clusters, statistical distributions in cluster shape and orientations at least in the plane of the film (which is the x - y plane in our case) are obvious, so that the simple equation for the Maxwell Garnett model (Figure 2) is not expected to describe realistic metal island films such as are obtained from evaporation processes in vacuum conditions. Instead, the statistical character of the island film geometry should be taken into account. In cases when the statistical distribution of the L -factors $g(L)$ is known, the effective dielectric function of the mixture can be calculated by a generalization of the Maxwell Garnett model according to:

$$\epsilon_{\text{mixture}} = \epsilon_{\text{host}} \frac{1 + \frac{p_{\text{guest}}(1-L)(\epsilon_{\text{guest}} - \epsilon_{\text{host}})}{\epsilon_{\text{host}} + (\epsilon_{\text{guest}} - \epsilon_{\text{host}})L}}{1 - \frac{p_{\text{guest}}L(\epsilon_{\text{guest}} - \epsilon_{\text{host}})}{\epsilon_{\text{host}} + (\epsilon_{\text{guest}} - \epsilon_{\text{host}})L}} \frac{\int_0^1 g(L) dL}{\int_0^1 g(L) dL} \quad (6)$$

Figure 6 sketches several assumed distributions of the L -factors for hypothetical model systems built up from spheres, needles and pancakes, as defined in Figure 6. Moreover, in Figure 6, corresponding ‘in-plane’ effective optical constants are shown as calculated by means of Eqs. (3) and (6) for several assumed filling factors, postulating in-plane optical isotropy of the whole film according to:

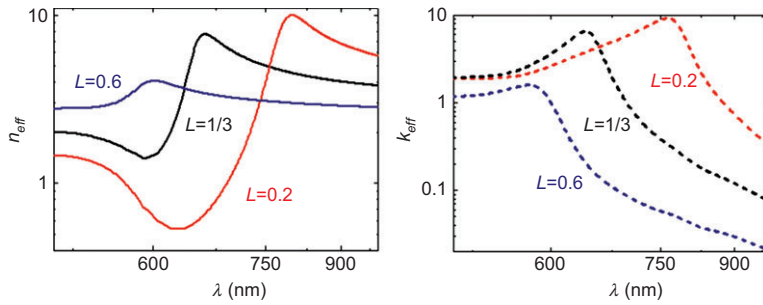


Figure 4 Simulated effective optical constants of a copper-alumina composite for different assumed depolarization factors. Simulation was performed in terms of the Maxwell Garnett model and a filling factor of 0.5.

$$g(L) = \frac{1}{2} [g_x(L_x) + g_y(L_y)] \quad (7)$$

Here g_x and g_y are the distributions of depolarization factors L_x and L_y , when the x -axis and y -axis correspond to main axes x and y of the individual ellipsoids (Figure 3), which are assumed parallel to the island film plane (Figure 2).

In Figure 6, alumina is again taken as the matrix (host) material, whereas copper serves as the island (guest) material. Except for the assembly of spherical clusters, the simulations result in rather broad absorption structures, which are obviously obtained as a superposition of the contributions of clusters with different depolarization factors. In fact, the broader the distribution in L is, the broader appears the absorption line. This leads to what is called an inhomogeneous broadening of the absorption line. Nevertheless, the picture still resembles the qualitative behavior of optical constants as described in terms of an oscillator model.

This is a rather powerful demonstration of the physical consistency of optical material models. What we did was take the bulk optical constants from alumina and

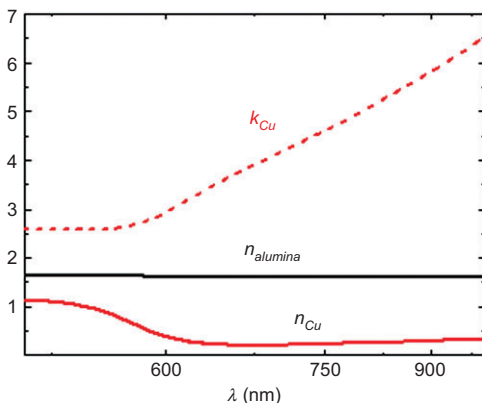


Figure 5 Optical constants of alumina and copper used for the simulation shown in Figure 4. For alumina, the extinction coefficient was set equal to zero.

copper from Figure 5 and calculate those of their mixture in terms of Eq. (6). From this, we obtained the resonance behavior which we had expected at the very beginning. We therefore conclude from these model calculations that it makes sense to model the effective optical constants of experimentally prepared metal island films in terms of an oscillator model. To take the mentioned inhomogeneous broadening effects into account, the so-called ‘multi-oscillator model could be the theoretical approach of choice to fit the measured optical spectra of real metal island films. This is the main conclusion from the simulations concerning the methodology of optical characterization of such island films.

Let us make one last remark concerning optical anisotropy of metal island films. So far we have discussed possible anisotropy as being caused from non-spherical cluster shapes. In fact, optical anisotropy of metal island films also appears as a consequence of the planar arrangement of the clusters. The point is that any optically excited cluster ‘feels’ the field scattered by its neighbors. This leads to coupling effects, which depend on the angle formed between the direction of the electric field vector and the island film plane. As a consequence, optical anisotropy may be observed even when the clusters are ideally spherical by shape. In Figure 7, possible mechanisms leading to optical anisotropy are visualized. In the design section, we will mainly focus on normal incidence specifications to avoid difficulty with anisotropy.

3 Experimental examples

3.1 A few words on experimental methods

Before coming to experimental methods, let us recall that our primary idea is to discuss metal island films as a substantial part of optical interference coatings. Although

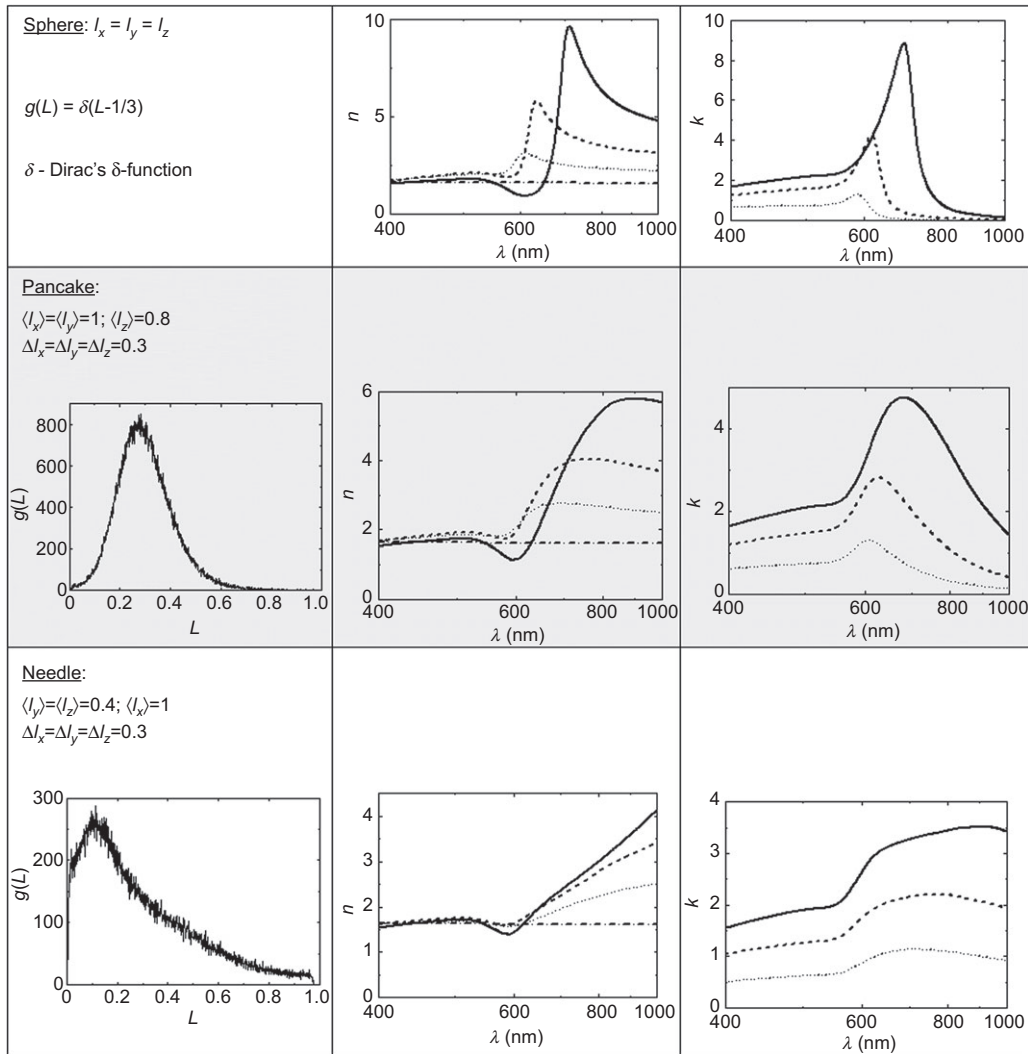


Figure 6 (Left) Assumed distribution of clusters with regard to depolarization factors. All length data are given in arbitrary units. (Right) Simulated by Eq. (6), dispersion of effective optical constants of copper-alumina composites for different filling factors (solid: $p_{\text{guest}}=0.6$; dash: $p_{\text{guest}}=0.4$; dot: $p_{\text{guest}}=0.2$; dash-dot: $p_{\text{guest}}=0$).

numerous methods are documented for the preparation of cluster materials [1, 14], only few of them are really compatible with the technology which is in practical use today for commercial interference coating preparation. This is schematically illustrated in Figure 8. We will therefore restrict our attention to experimental methods which are at the same time compatible with clusters science as well as with coating technology. Nevertheless, available scientific literature devoted to the preparation of metal island films has grown to unmanageable quantities, which might be an indication of both the scientific interest devoted to metal island films as well as the relative simplicity to prepare them by physical vapor deposition (PVD) methods. Just for fun, the reader is recommended to perform a Google search using search criteria such as

‘metal island film evaporation’ or ‘metal island film sputtering’ to get an impression of the huge number of hits.

The good news from such a literature search is that metal island films may obviously be prepared by both evaporation and sputtering techniques, so that the main preparation techniques used for optical coating production today are compatible with the preparation of metal island films. For this tutorial, we will use practical examples which stem from evaporation of metals in high vacuum conditions. Technical details are published in [15, 16]. Generally, when preparing metal island films by evaporation, the classical rule ‘quick and cold’, which is important for obtaining high quality closed metal films, should be reversed. Rather regular island films are obtained with a low deposition rate on heated substrates. One example

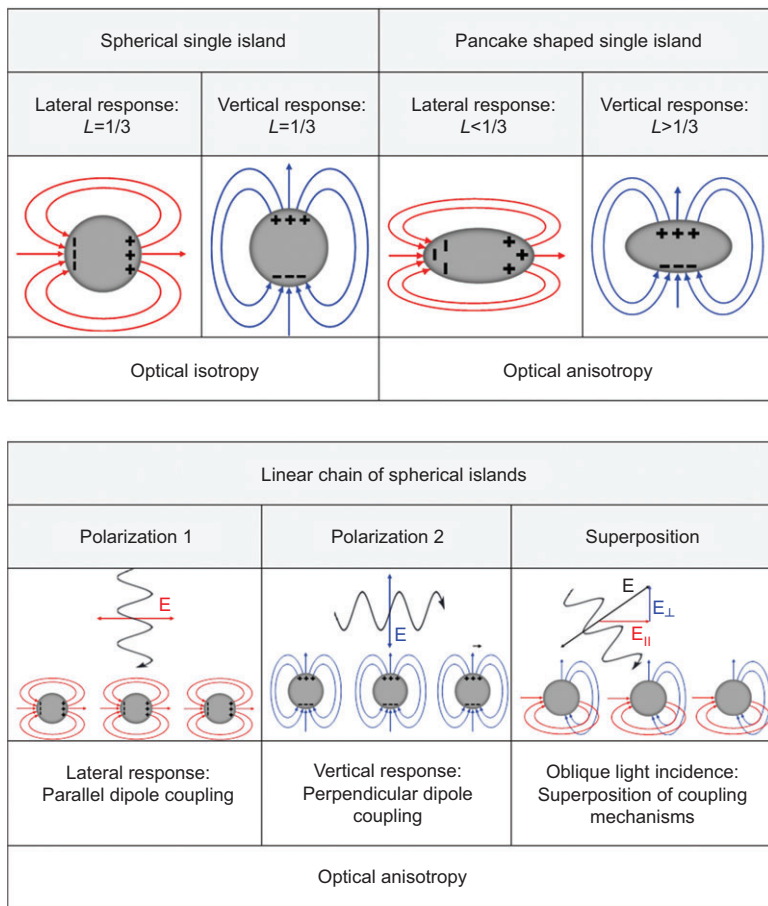


Figure 7 Illustration of possible reasons of optical anisotropy in metal island films. Note that in practice the wavelength is much larger than the cluster dimensions.

of the effect of the substrate temperature on the properties of a metal island film will be given in section 3.3.

Concerning film characterization, metal island films turn out to be accessible to both spectrophotometric and spectroellipsometric measurements, as shown by relevant

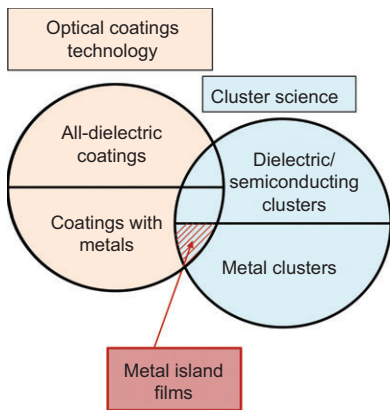


Figure 8 Status of metal island films as an interface between optical coating technology and cluster science.

studies [17, 18]. In this regard, full compatibility to conventional coating characterization technology is also guaranteed. Nevertheless, as already indicated in the introduction section, more sophisticated mathematical approaches have to be applied to perform a successful reverse search procedure (i.e., determining effective optical constants from measured spectra). Any type of side information on the coating thickness and/or morphology, as accessible, for example, from electron microscopy is extremely helpful in obtaining reliable results.

Below we will present two examples on metal island films as deposited by thermal evaporation. In the first example, copper island films are embedded in an alumina matrix. In this example, we study samples with a different amount of evaporated copper, while all other deposition conditions are kept the same. In the second example, silver clusters are incorporated again in an alumina matrix. But in this case, the evaporated amount of metal is the same for all samples, while it is the substrate temperature which has been varied. We will highlight and discuss the corresponding changes in the effective optical

constants of the island films. In section 4, several design ideas will be proposed to highlight possible applications of such films.

3.2 Example 1. Copper island films in alumina: dependence of the effective optical constants on the amount of copper

As practical examples, we will make use of experimental data published in earlier studies [15, 16]. Hereby, in study [15], copper island films have been investigated, while [16] is focused on silver island films.

According to [15], copper island films were deposited by thermal evaporation in a Leybold A1200 deposition system, equipped with quartz crystal monitors. The substrate temperature was set to 90°C. Seven fused silica slabs for optical characterization as well as seven fine copper grids coated with a 10-nm thick amorphous carbon film (supplied by PLANO GmbH, Wetzlar, Germany) suitable for subsequent film characterization by transmission electron microscopy (TEM) were used as substrates.

The films with different mass coverage have been deposited in essentially one deposition run. To guarantee an identical dielectric environment for each of the films, deposition started with an approximately 5–6 nm thick alumina film, deposited by electron beam evaporation. Next, copper deposition by thermal evaporation was started until a certain quartz monitor signal was reached, which was expected to correspond to approximately 1.7 nm copper equivalent. Then, the first sample was shadowed to prevent it from further deposition. The deposition process was continued until twice the monitor signal was reached, then shadowing the second sample, and so on. This way a scale of copper film thicknesses was realized, corresponding to the values given in Table 2. Finally, all samples were again exposed to the deposition to cover

Sample number j	$d_{\text{Al}_2\text{O}_3} + d_{\text{Cu}} + d_{\text{Al}_2\text{O}_3}$ (nm)	Copper filling factor p_{guest} in vol.% estimated according to $p_{\text{guest}} = 100\% * d_{\text{Cu}} / (2d_{\text{Al}_2\text{O}_3} + d_{\text{Cu}})$
1	13.5	12
2	15	22
3	16.5	30
4	18	37
5	19.5	43
6	21	48
7	37.9	–

Table 2 Description of the copper island films.

Note that samples 1 and 6 will be used in design calculations later in section 4.

them with another 5–6 nm thick alumina film. As a result, a set of island films with the same alumina thickness, but with different copper thicknesses, was available for both optical and TEM characterization.

The deposition of each of the island films numbered by j ($j=1 \dots 7$) therefore consists of three steps: alumina (matrix) deposition, copper (metal) deposition and alumina (matrix) deposition. Each of these samples has a full metric thickness corresponding to the data from Table 2, and is characterized by a set of effective optical constants which should describe its optical behavior in accordance with the given thickness.

From *ex situ* normal incidence transmission and reflection spectra of the single films on fused silica and the thickness known from Table 2, the effective optical constants for each of the films 1–7 were calculated by means of a spectra fit in terms of a Lorentzian multi-oscillator model (compare conclusions from section 3). In the electric dipole approximation, these effective optical constants are valid for any experimental geometry where the electric field vector is parallel to the island film plane. In Figure 9, the thus obtained effective optical constants of the copper island films are visualized. Particularly in

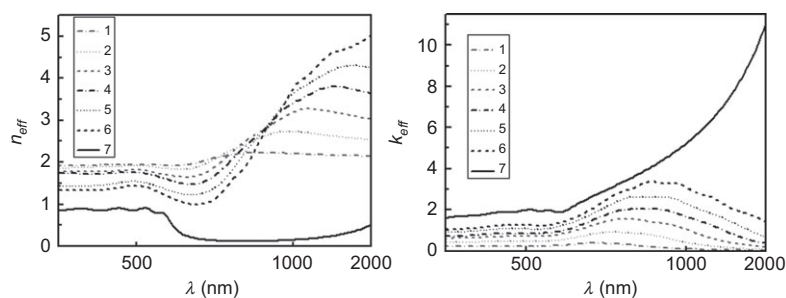


Figure 9 Effective optical constants of the copper (island) films 1–7, as obtained from normal incidence transmission and reflection spectra.

the extinction coefficients of samples 1–6, a rather broad resonance structure may be identified, which shows an increase in integral intensity, width and maximum wavelength with increasing copper coverage. Qualitative similarity to the modeled effective optical constants shown in Figure 6 is thus clearly observed. This is a rather typical behavior for excitation of localized surface plasmons in metal island films in a dielectric environment [1]. On the contrary, the thickest film 7 (i.e., the copper island film with the highest thickness) shows effective optical constants which are already close to those of bulk copper (compare Figure 5 and Figure 1 on the right), indicating that this film is already closed.

At the same time it should be noted that according to the data given in Table 2, each of those island films has another thickness. In fact, any of the sets of effective optical constants in Figure 9 is tightly connected to a certain deposition procedure and a well-defined thickness. Thus, it makes no sense to discuss an island film with the effective optical constants from sample 4 and a thickness of, for example, 25 nm, because it cannot be manufactured. This must be kept in mind when performing design calculations with metal island films.

The reason becomes clear from looking at Figure 10, where the corresponding TEM images are summarized except sample 3, which was damaged during handling.

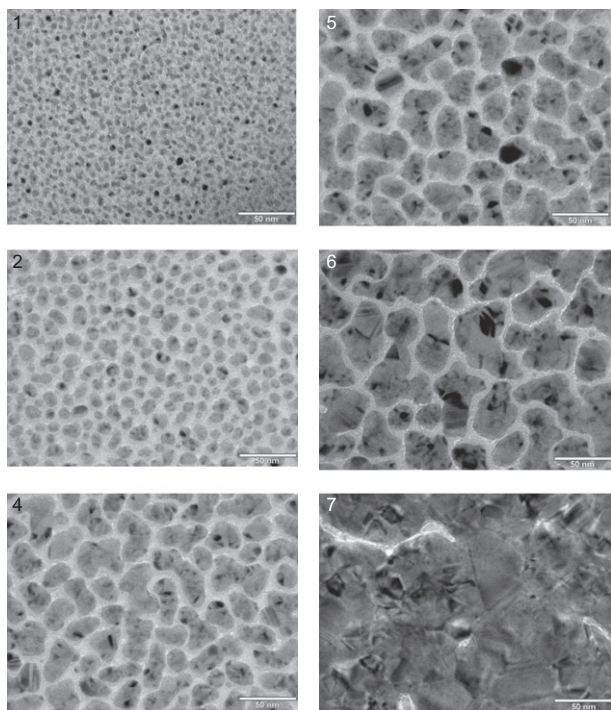


Figure 10 Lateral TEM images of the copper (island) films 1–2 and 4–7. The bar on the right on the bottom of each image corresponds to a length of 50 nm.

Nevertheless, the images confirm the presence of isolated copper islands (the dark regions) in samples 1–6, whereas in sample 7 the islands have clearly percolated to form a rather closed copper film. With increasing coverage, the islands tend to become larger and more irregular in shape. Thus, it is not only the filling factor which is changed when the amount of copper is increased but also the shape of the clusters. This results in distributions of depolarization factors which in turn depend on the filling factor p_{guest} . Thus, filling factor and cluster shapes appear mutually interconnected, and therefore, at least by means of evaporation techniques, thickness and effective optical constants cannot be adjusted independently from each other.

It might seem from the presented ‘top views’, that the cluster shape tends to approach spherical symmetry when the copper thickness is rather low. However, when keeping the deposited amount of copper in mind, it appears clear that those clusters should rather be tackled as oblates or pancakes. Moreover, a glance at the effective optical constants modeled in Figure 6 confirms that even the optical behavior of the low-copper coverage samples is not consistent with the assumptions of spherical clusters, but rather with that of pancakes. At higher coverage, the experimental effective optical constants are rather in agreement with simulations based on the assumption of an assembly of needle-like clusters.

In summary, from the presented data we learn that an increase in the amount of the deposited (by evaporation) metal is accompanied by an increase in the integral absorption, as well as a broadening and red-shift of the plasmon resonances.

3.3 Example 2. Silver island films in alumina: dependence of the effective optical constants on the deposition temperature

In this example, the dielectric matrix material is the same as before (alumina), whereas the clusters are now built from silver and the material amount is identical in all systems. Sample deposition was started with an alumina underlayer (3 nm), followed by silver corresponding to a mass coverage of 4 nm, and followed by an alumina overlayer (3 nm) [16]. The silver filling factor is therefore approximately 40% in all samples, whereas the latter differ in their deposition temperature, which was varied between 20°C and 300°C. The effect of the deposition temperature is visualized in Figure 11 and 12.

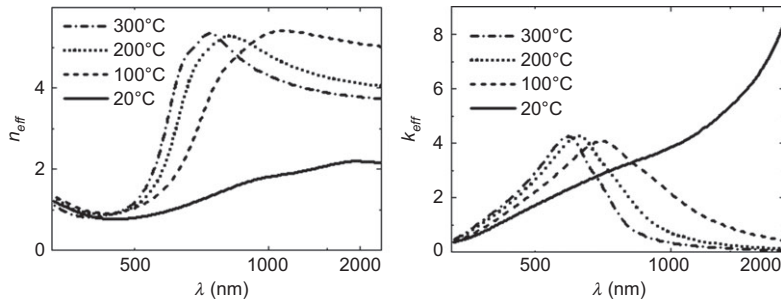


Figure 11 Effective optical constants of the silver island films, as obtained from normal incidence transmission and reflection spectra.

In particular, from looking at the TEM images (Figure 12), it appears that the deposition temperature again has an effect on the shape of the clusters; at higher temperatures the clusters appear less distributed with respect to size and shape. Again, the samples with well-segregated clusters (deposition temperature 100°C and higher) show a resonance behavior in the extinction coefficient, which can be attributed to the silver surface plasmon resonance in alumina. The distribution with respect to the cluster shapes results in a decrease in resonance wavelength and spectral width with increasing temperature. In contrast to the example in Figure 9, integral absorption seems almost the same for all samples, except the percolated sample (deposited at 20°C). This suggests that a check of integral absorption gives access to the

metal filling factor of the samples, which changes from sample to sample in Figure 9, but is rather constant for the samples in Figure 11.

In fact, there exists a correlation between filling factor of the metal fraction and integral absorption (a so-called sum rule [13]). Again, in its theoretically strong version it must be expressed in terms of dielectric function:

$$p_{\text{guest}} \propto \int_0^{\infty} \text{Im} \varepsilon_{\text{mixture}}(\omega) \omega d\omega \propto \int_0^{\infty} n_{\text{eff}}(\omega) k_{\text{eff}}(\omega) \omega d\omega \propto \int_0^{\infty} n_{\text{eff}}(\lambda) \frac{k_{\text{eff}}(\lambda)}{\lambda} d\frac{1}{\lambda} \quad (8)$$

As long as the absorption feature is spectrally narrow and centered around some wavelength λ_0 , and the refractive index is rather constant, the following approximation holds:

$$p \propto \frac{n_{\text{eff}}(\lambda_0)}{\lambda_0} \int_{\lambda_0 - \Delta\lambda}^{\lambda_0 + \Delta\lambda} k_{\text{eff}}(\lambda) d\frac{1}{\lambda} \quad (9)$$

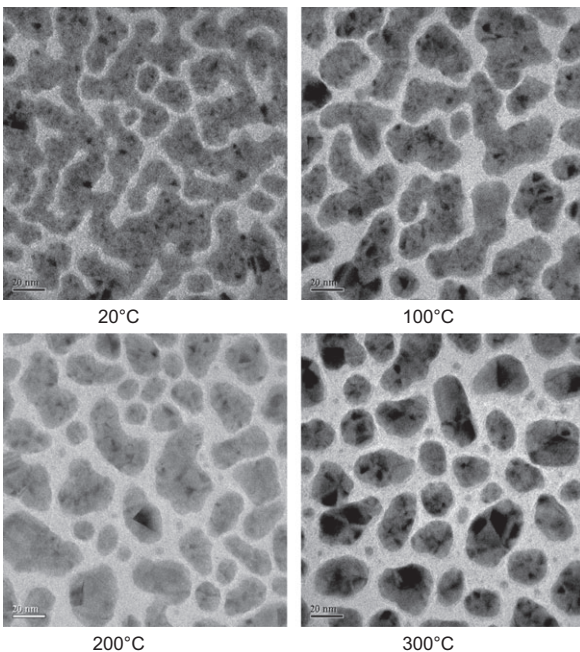


Figure 12 Lateral TEM images of the silver island films. The bar on the left on the bottom of each image corresponds to a length of 20 nm.

In this special case, filling factor really scales with the integral over k_{eff} in a reciprocal wavelength scale. But these conditions are obviously no longer fulfilled for the 20°C sample from Figure 11, and therefore filling factor is directly determined by Eq. (8). This is finally illustrated in Figure 13, where instead of k_{eff} the value $n^*k_{\text{eff}}/\lambda$ (the ‘integrand’) is plotted over the wavelength (again in reciprocal scaling). In this presentation, obviously, the integral ‘absorption’ from ‘zero’ to ‘infinity’ might really be similar for all four samples.

This was an example on four metal island films, which have the same thickness as well as the same filling factor. Nevertheless, the effective optical constants are drastically different, because of the differences in the shapes of the clusters caused by different deposition temperatures. Again, every film needs its ‘own’ effective optical constants to be correctly described.

In concluding this section, we therefore emphasize that the optical behavior of metal island films may be

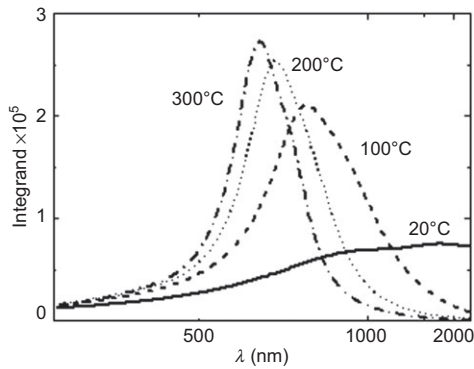


Figure 13 The term $\frac{n_{eff}(\lambda)k_{eff}(\lambda)}{\lambda}$ as a function of wavelength for the silver island films.

described by so-called effective optical constants, which makes them accessible to conventional thin film design strategies. But the price for introducing these effective optical constants is their thickness dependence. The thickness of a metal island film must not be varied during a design procedure. A metal island film with given thickness and given effective optical constants has to be tackled as a fixed building block which can be introduced into an interference stack, but should not be modified during synthesis and refinement.

4 Design considerations with metal island films

In our familiar designs of optical coatings we make much use of dielectric materials, that is, materials with extinction coefficients close to zero. We also make use of high-performance metals such as silver that are characterized by a large extinction coefficient but a very small refractive index. These situations correspond to what is shown in the long wavelength edges in Figure 1. The composite materials that we consider here are rather different in that both the index and extinction coefficient are significant. This limits their use in traditional coatings but also opens up new possibilities. A limitation that is missing from normal coating design is the strict constraint on the thickness of the composites and this is something that we must accept. Our designs, therefore, will largely be tailored to make use of the novel optical constants of the materials. We will not have the same facility of shifting the performance in wavelength simply by changing the reference wavelength that we have in the traditional methods. We begin by surveying some existing theory.

4.1 Potential transmission

The concept of potential transmission dates back to the classical paper of Berning and Turner [19]. It is deceptively simple but is one of the most powerful concepts we have. For a complete derivation of what we use here see, for example, [20]. Transmittance is defined, effectively, as what emerges compared with what is incident. Potential transmittance is what emerges compared with what actually enters. In a coating with transmittance T and reflectance R potential transmittance, ψ , is given by:

$$\psi = \frac{T}{(1-R)} \tag{10}$$

This form of the definition presents a problem when the incident medium is absorbing, or when we are looking at individual layers in a system that may or may not be absorbing and thus a more useful definition in that case is:

$$\psi = \frac{\text{Re}(y_{sub})}{\text{Re}(BC^*)} \tag{11}$$

where y_{sub} is the characteristic admittance of the emergent medium and B and C are the corresponding normalized tangential electric and magnetic amplitudes at the entrance surface. At oblique incidence y_{sub} becomes the appropriate tilted admittance η_{sub} .

It can readily be shown that:

$$\psi = \psi_1 \psi_2 \psi_3 \psi_4 \dots \tag{12}$$

Because a completely dielectric film has no loss, its potential transmittance is necessarily unity. Thus, the potential transmittance of a system of layers will be the product of the potential transmittance of the absorbing layers only. If there is only one absorbing layer then the potential transmittance of the entire system will be that of that single layer.

Let us concentrate for the moment on one absorbing layer in some structure. Let the surface admittance presented at the rear of the layer be given by Y_{exit} . Then the potential transmittance will be given by:

$$\psi = \frac{\text{Re}(Y_{exit})}{\text{Re}(BC^*)} \tag{13}$$

but once the thickness and optical constants of the film are specified, B and C are immediately known and depend only on Y_{exit} . This implies that, once a layer is defined, its potential transmittance depends only on Y_{exit} . Clearly, it is impossible to achieve a potential transmittance of unity (or 100%) from a layer that suffers from absorption. However, because the potential transmittance depends of Y_{exit} , it is

possible to find a value such that potential transmittance is maximized. The analysis is straightforward but extremely tedious and the analytical expressions for the optimum Y_{exit} and the maximum potential transmittance rather involved. They are given, for example, in [20]. In physical terms, what the optimization does is to minimize the electric field throughout the layer so that the absorptance is limited. This maximizes the potential transmittance. To achieve an actual transmittance equal to the potential transmittance it is necessary first to construct a system of lossless layers at the rear of the absorbing layer to present the optimum surface admittance. Because the layers are lossless, the potential transmittance of the matching assembly will be unity. Then finally, once the optimum potential transmittance is achieved a matching system of lossless layers must be added to the front surface of the absorbing layer to reduce the reflectance to zero. This second operation is rendered easier by the fact that the admittance presented by the outer surface of the absorbing layer is necessarily the complex conjugate of the optimum exit admittance. A filter constructed according to this prescription is known as an induced transmission filter and such filters, using silver as the absorbing layer, are readily available commercially.

Although such maximizing operations are readily performed at one single wavelength, it is much more difficult, if not impossible, to achieve this result over a wider wavelength region. The principal reason is the considerable variation with wavelength in the value of the optimum exit admittance that is essentially opposite to the sense of variation readily achieved by a dielectric system. Taking our 21-nm copper island film (see Table 2) as the subject, the potential transmittance as a function of wavelength is shown in Figure 14.

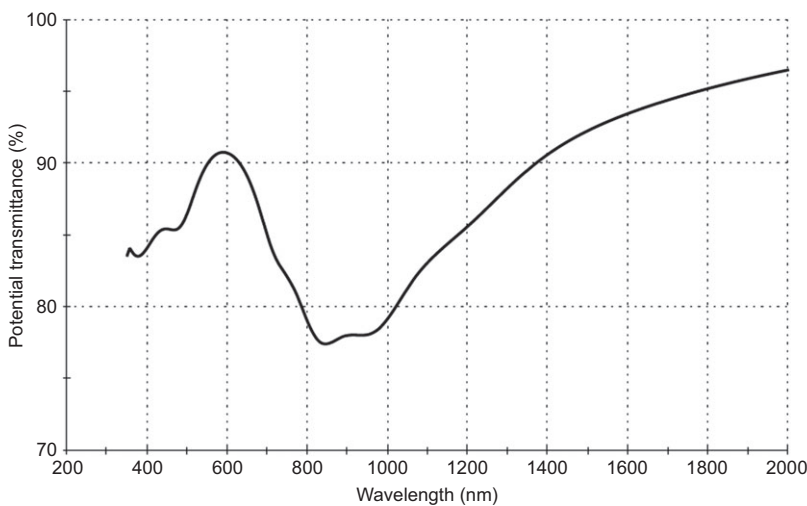


Figure 14 The optimum potential transmittance of the 21-nm copper island film as a function of wavelength.

Figure 15 shows the locus of the optimum value of Y_{exit} as a function of wavelength. The exceedingly steep rise with increasing wavelength is impossible to match with a straightforward dielectric system. Dielectric layers exhibit a shortening locus with increasing wavelength, exactly the opposite of the sense of variation in Figure 15. It should not be thought that this behavior is a consequence of the dispersion of the properties of the absorbing layer. Even absorbing materials with properties that are completely stationary with varying wavelength exhibit a rather similar variation in the optimum admittance. We note that this has always been a problem with traditional silver-based induced transmission filters.

Let us construct an induced transmission filter using a 21-nm thickness of the composite material. We choose 600 nm as the wavelength for optimization. For simplicity, let us use dispersionless lossless materials for the other parts of the design, 1.52 for the substrate index and for that of the incident medium (we will assume that this represents a cemented cover), and then 1.45 and 2.15 for the indices of the two types of dielectric layers. The optimum exit admittance is $3.8937 + i6.9068$ and the corresponding optimum potential transmittance is 90.73%.

Let us arrange that the layer next to the copper composite is the high-index 2.15. In the normal way the matching structures are arranged to consist of a series of quarter-waves with a phase matching fractional thickness layer next to the metal when the metal thickness may be varied slightly so that the match is as near perfect as possible. Here we must retain the 21-nm thickness of the composite material, otherwise the effective optical constants shown in Figure 9 will be incorrect. To accommodate this, the phase matching must now be a two-layer system, a small

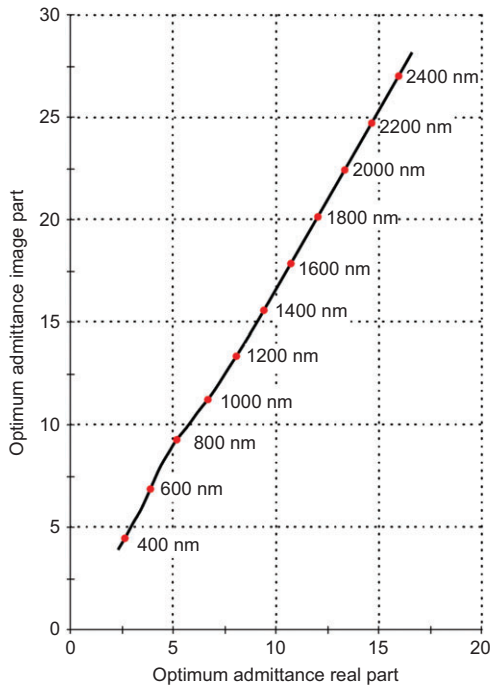


Figure 15 The optimum exit admittance for the 21-nm copper island film.

complication. A judicious starting system with some automatic adjustment yields the design:

1.52|HLHLH 0.236L 1.514H M 1.514H 0.236L HLHLH|1.52 with $\lambda_0=600$ nm

where the symbol M indicates the composite layer.

The resulting performance (Figure 16) shows the expected peak transmittance and the narrowband form of the performance but the rejection is poorer than we would expect with a closed silver metal layer.

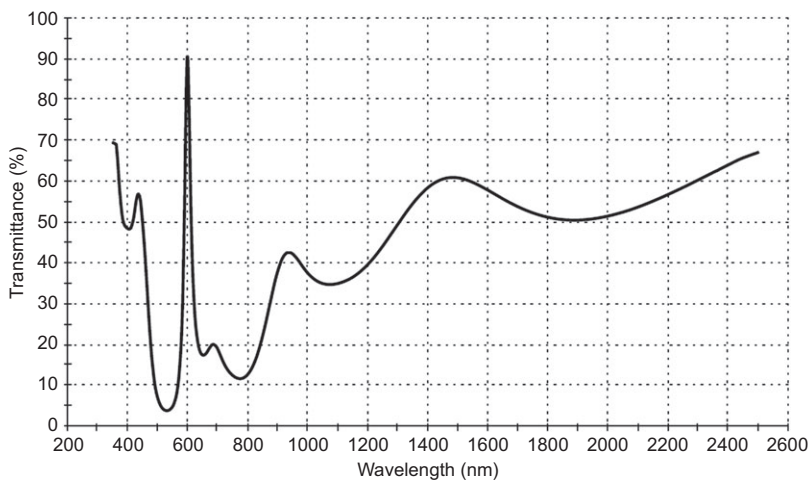


Figure 16 The performance of the induced transmission filter. The estimated peak transmittance is achieved but the overall performance is discouraging.

4.2 Potential absorption

A different design direction is afforded by attempting to increase absorptance and here the concept of potential absorption is useful.

Potential transmittance is a measure of the throughput of the system as a function of the actual input. Potential absorptance, \mathcal{A} , is a measure of what is lost in the system as a function of the actual input. Clearly,

$$\mathcal{A} = 1 - \psi = \frac{A}{(1-R)} \tag{14}$$

where A is the absorptance. Rather like potential transmission, the concept of potential absorption is more amenable to analysis.

Potential absorptance has a minimum value corresponding to the maximum value of potential transmittance but it does not have a clear maximum. In the induced transmission filter of Figure 16, the potential absorptance at the peak of the filter is the minimum possible for the composite layer. However, this is not particularly useful because the actual absorptance can be further reduced simply by increasing the reflectance.

Rather like potential transmittance, the analysis of potential absorptance is tedious and involved and the expressions are too complicated to lend themselves to ready interpretation. However, a very useful result can be derived [20] assuming that the thickness of the absorbing layer, d , is very small.

$$\mathcal{A} = \frac{4\pi nkd}{\lambda} \frac{1}{\text{Re}(Y_{\text{exit}})} \tag{15}$$

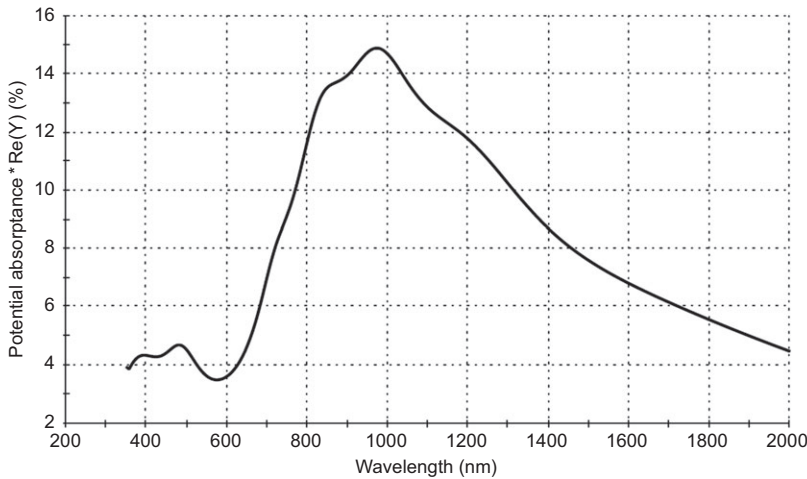


Figure 17 The potential absorbance of a 1-nm thickness of the 21-nm copper composite for an exit admittance of unity. This is equivalent to $4 \pi nk/\lambda$.

This could be a thin slice of a thicker layer. It helps us to understand the variation of absorption in an admittance locus. This expression indicates that to enhance the absorption in the layer we should position it in the admittance diagram as close to the imaginary axis as possible.

Note that the term nk/λ in Eq. (15) is nothing more than the integrand in the sum rule Eq. (8) (see also Figure 13). Therefore, for single ultrathin composite layers, the ‘integral’ potential absorbance appears to be directly proportional to the product of the metal filling factor p_{guest} and the island film thickness d . This is an important monitoring issue, because both these parameters have to be controlled in a deposition process. Once from Eq. (10) and Eq. (14) it follows that:

$$A = 1 - \psi = \frac{A}{(1-R)} = 1 - \frac{T}{(1-R)} \tag{16}$$

in situ control of spectral transmittance T and reflectance R of a single metal island film gives direct access to the product of filling factor and thickness without any complicated numerical re-engineering procedure. Indeed, combining Eqs. (8), (15) and (16) we find:

$$p_{\text{guest}} d \propto \int_{\lambda_{\text{min}}}^{\lambda_{\text{max}}} \left\{ 1 - \frac{T(\lambda)}{[1-R(\lambda)]} \right\} \frac{\text{Re}Y_{\text{exit}}(\lambda)}{\lambda^2} d\lambda \tag{17}$$

The application of Eq. (17) makes sense as long as the available spectral range $[\lambda_{\text{min}}, \lambda_{\text{max}}]$ contains a major absorption feature of the guest fraction, while the dielectric host may be regarded as non-absorbing in that range. When monitoring is performed on a weakly dispersive witness glass, the exit admittance is rather constant, and we find:

$$p_{\text{guest}} d \propto \int_{\lambda_{\text{min}}}^{\lambda_{\text{max}}} \left\{ 1 - \frac{T(\lambda)}{[1-R(\lambda)]} \right\} \frac{d\lambda}{\lambda^2} \tag{18}$$

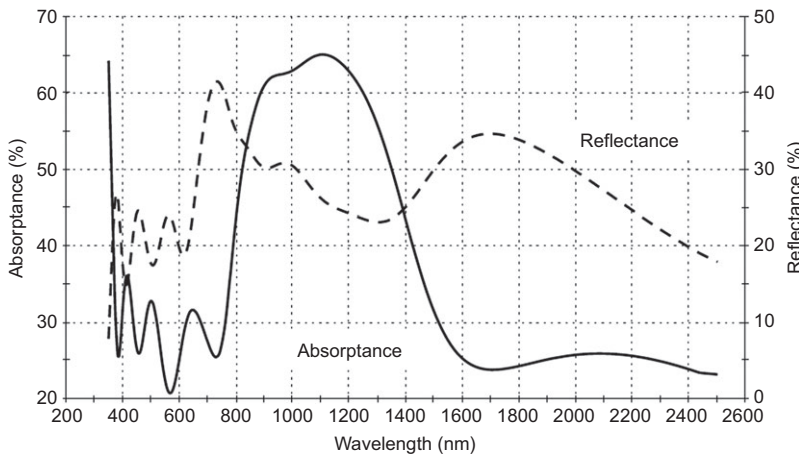


Figure 18 The absorbance and reflectance of the preliminary coating. The reflectance at 30% is a little too high.

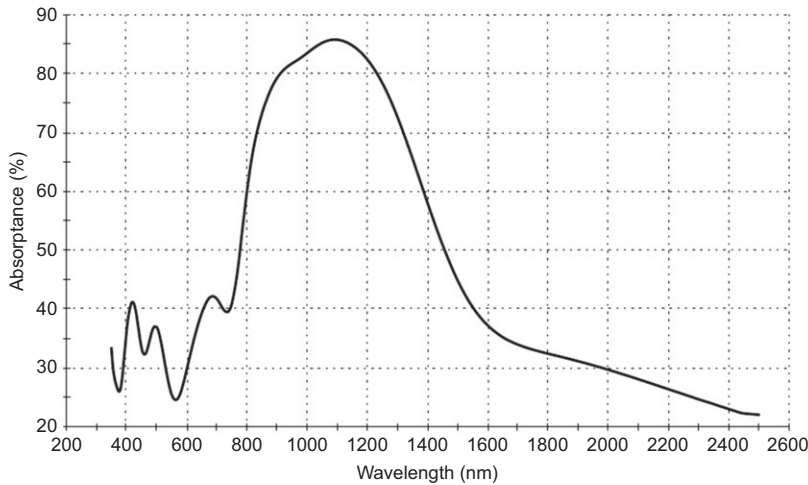


Figure 19 The anti-reflection coating has increased the absorbance up to 85%.

But let us return to our absorber design problem. The function $4\pi nk/\lambda$ for the 21-nm copper composite is shown in Figure 17. Clearly, the region around 1000 nm is most attractive for enhancing absorbance.

We first reduce the exit admittance, Y_{exit} , to 0.314 at 1000 nm by a simple system of quarter-wave layers, and then place a 21-nm copper composite over it.

M LHLH | 1.52

The performance of the system at this stage is illustrated in Figure 18. The reflectance at around 30% is perhaps a little too high and we need to anti-reflect the system.

We would like to accomplish this over as wide a spectral region as possible but the design is complicated by the variation of admittance of the structure. We therefore choose the region 400–1500 nm and adopt an automatic

technique. We do not wish to complicate the design needlessly and thus we adopt a four-layer system that finally yields the following design.

Air| 0.7858L 0.2208H 0.1761L 0.6283H M LHLH | 1.52 with $\lambda_0=1000$ nm.

The final performance is shown in Figures 19 and 20. The coating transmittance is that of a near infrared rejection filter, but rather than being reflected the infrared is absorbed.

4.3 Neutral density filters

Neutral density filters are commonly based on lossy metals such as chromium, Inconel (an alloy with nickel and chromium as primary components and a registered trademark

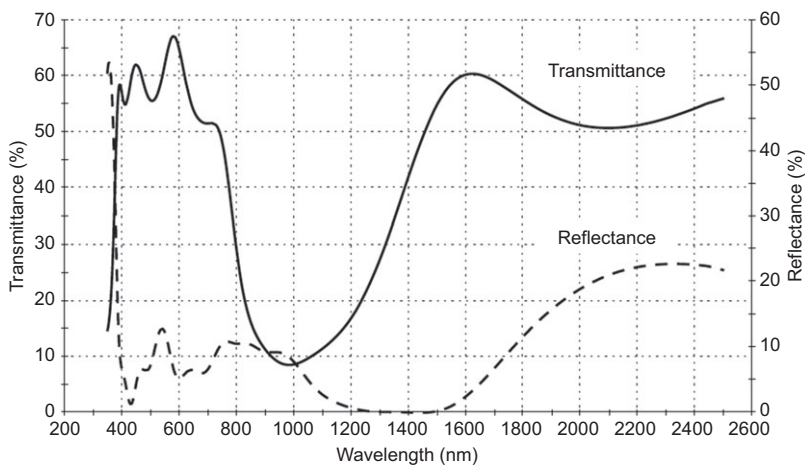


Figure 20 The transmittance and reflectance of the completed design. The visible region is transmitted with some absorption loss and the near infrared is almost completely absorbed.

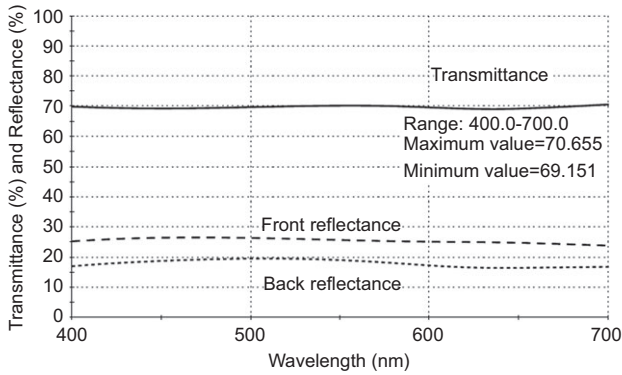


Figure 21 The performance of a neutral density filter based on the 13.5-nm composite layer. The label shows the range of transmittance. The design has collapsed to Air | M (13.5 nm) L (44.88 nm) | 1.52.

of Special Metals Corporation, Huntington, USA) or nichrome (an alloy of nickel, chromium and sometimes iron). The question then arises whether the present composite materials could be useful in neutral density filters. We shall concentrate on the visible region, 400–700 nm. The metals mentioned are frequently deposited as single layer coatings, although sometimes an anti-reflection coating on the outer surface may be added to avoid stray reflected light. Tolerances are rarely discussed but there can frequently be a variation of several percent in transmittance over the visible region. We shall concentrate on flattening the characteristic as far as possible rather than reducing the reflectance.

The simple basic design that we shall use consists of the following where M indicates the composite layer:

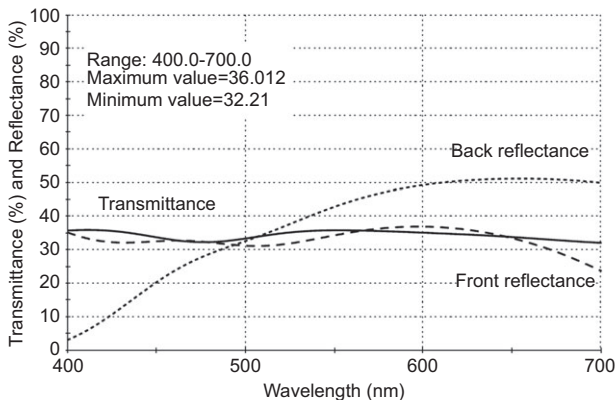


Figure 22 The performance of a neutral density filter based on the 21-nm composite layer. Here the dispersion of the material does not permit quite as flat a performance as in Figure 21. Further flattening requires a more complex design. Again the label shows the range of transmittance. The final design is: Air | H (50.17 nm) L (34.35 nm) M L (106.39 nm) H (22.86 nm) | 1.52.

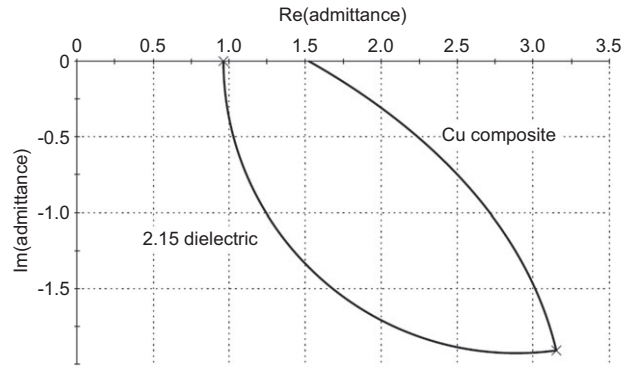


Figure 23 The admittance diagram for the forward direction in the two-layer beamsplitter.

Air | H L M L H | 1.52 (glass)

The H and L symbols represent indices of 2.15 and 1.45, as before, but they are not necessarily quarter-waves, but have thicknesses chosen to flatten, as far as possible, the characteristic. The system at the rear is intended largely to modify the potential absorptance, whereas the system at the front adjusts the reflectance. Because we cannot control the thickness we shall take flatness as the primary criterion rather than a particular transmittance.

In the case of the thinnest composite layer (film 1 in Table 2), the design collapses to one matching layer in behind the composite layer (Figure 21). The other illustration (Figure 22) uses the most difficult layer, the 21-nm thick composite. Here the result is not quite as good but is still acceptable.

Tilting the neutral density filters shows little change for mean polarization but, as might be expected, there is some polarization splitting in the sense that *p*-transmittance is rising while *s*-transmittance is falling.

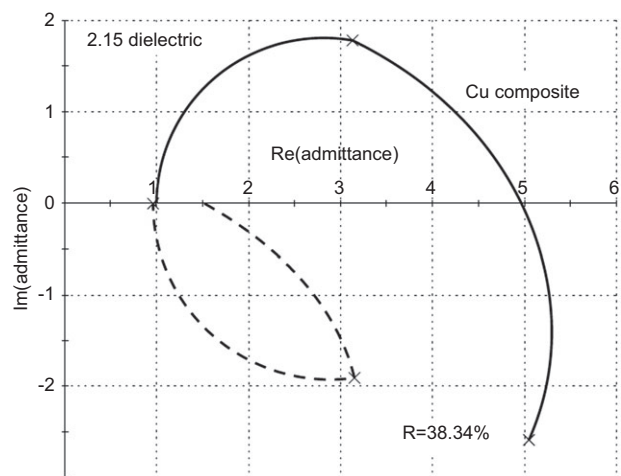


Figure 24 The admittance locus in the reverse direction compared with the forward one from Figure 23 (shown broken).

4.4 Asymmetric beamsplitter

An old problem is a beamsplitter that has zero reflectance on one side and as high a reflectance as possible on the other. With lossless layers it is impossible to construct such a coating. Transmittance is always symmetrical and without absorptance the reflectances on either side must be equal. Because transmittance is the same both ways the difference in reflectance from one side to the other is identical to the difference in absorptance. Note, however, that the transmittance can never be higher than the complement of the highest absorptance. Thus, there is a complicated balance between the various attributes of the beamsplitter. In such beamsplitters, simplicity is invariably chosen over optimum performance.

Let us design a simple beamsplitter of this type for 800 nm. We choose once again the 21-nm composite. The principle is given essentially in Eq. (15). $1/\text{Re}(Y_{\text{exit}})$ should be as different as possible in the forward and reversed directions. Let us take Y_{exit} for the composite layer in the forward direction as 1.52, as that layer will be next to the glass substrate. From an admittance locus it is fairly easy to see that a layer of index 2.15, some 0.763 quarter-waves in thickness is close to a perfect anti-reflection coating, Figure 23, which is a happy coincidence.

Now we reverse the order so that the light is propagating in the opposite direction. The dielectric layer will start at a surface of air and swing into the first quadrant so that the starting point for the composite layer is considerably displaced from the 1.52 admittance in Figure 23. This is shown in Figure 24. The reflectance at 800 nm in the reverse direction is 38.34%.

The forward reflectance is virtually zero (0.038%). The back, or reverse, reflectance is 38.34%. The transmittance

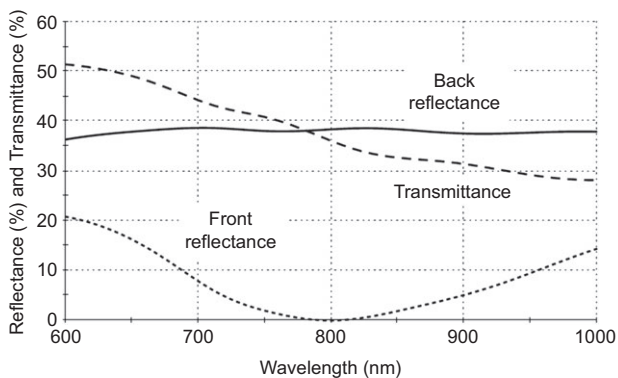


Figure 25 The performance parameters of the asymmetric beamsplitter.

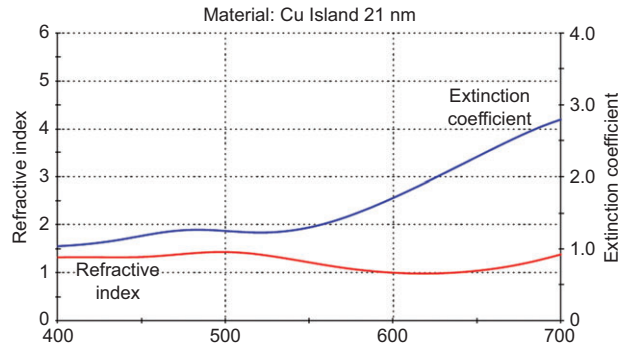


Figure 26 The effective optical constants of the 21-nm composite plotted over the visible region.

in both directions is 36.02%. Such beamsplitters require at least one absorbing layer and thus they suffer from absorption losses (Figure 25). This is fundamental and nothing can be done to remove the absorption. However, it is possible to flatten the characteristic a little but at the price of a much more complicated design. The same asymmetry is found in some coatings for reflecting sunglasses. The outer surface, visible to others, reflects, but this would be a problem at the inner surface where glare could be reflected into the eye and thus that surface has very low reflectance.

4.5 Decorative effects

Decorative coatings are almost invariably used in reflection. Transmittance is unimportant and is usually zero. The dispersion of the composite materials over the visible region (Figure 26) is not very different from that of the

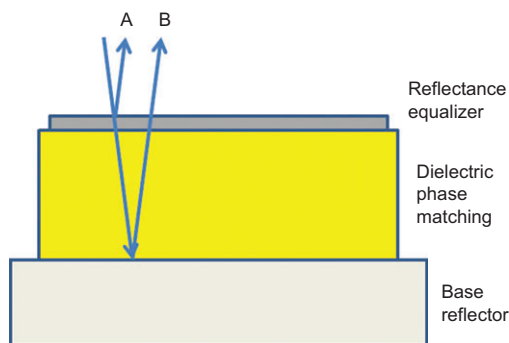


Figure 27 The structure of a simple reflecting decorative coating. The two reflected beams are equalized in amplitude by the front reflectance equalizer, usually a metal such as chromium, whereas the dielectric phase matching layer assures that the beams are in antiphase. The resulting anti-reflection fringe is arranged to be of a suitable width to suppress one of the primaries so as to give good purity to the color.

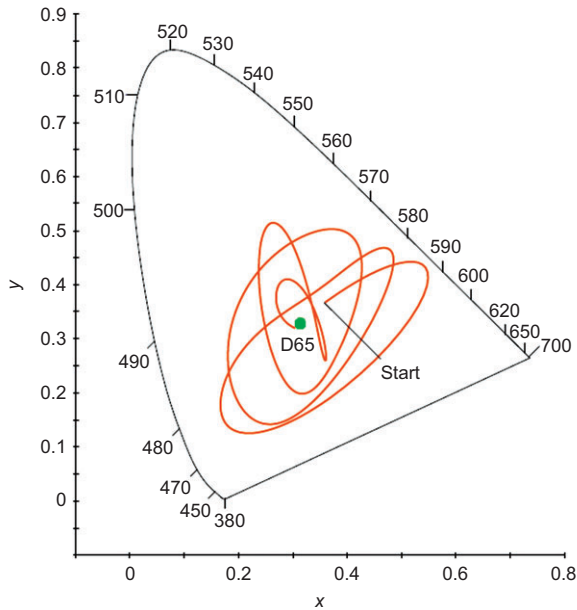


Figure 28 The range of chromaticities achievable with the 21-nm island film in the structure of Figure 27 and a phase matching layer of index 2.15 and varying in thickness from 0 to 500 nm. The CIE 1931 observer with illuminant D65 is used.

metallic films such as chromium that is frequently used in such coatings. The film therefore does not have an intrinsic color that would on its own support an intensely decorative film. Some interference effects are therefore required.

A typical structure uses a base of silver or aluminum, highly reflecting, over which is deposited a dielectric phase matching layer followed by a reflection equalizing film often consisting of chromium or a similar metal. In our case, we will use the 21-nm composite. The basic structure is shown in Figure 27. Adjustment of the thickness of the phase matching layer will alter the wavelength of the anti-reflection effect and hence vary the color.

A rather nice effect is a golden color given by the design:

Air | M (21 nm) H (116.3 nm) | Silver

The use of the high-index phase matcher ($n=2.15$) reduces color variation with angle of incidence and thus the coating presents a gold-like appearance even to fairly high angles of incidence.

The range of chromaticities achievable by varying the thickness of the phase matching layer from 0 to 500 nm is shown in Figure 28.

5 Concluding remarks

In concluding the main message of this tutorial, we would like to mark a few major points which seem to us essential when applying metal island films in optical coating practice.

- The optical response of metal island films may be described in terms of effective optical constants and a respective thickness. In this regard, these films are accessible to conventional thin film design and characterization software, where any layer is characterized by its thickness and a set of corresponding optical constants.
- The effective optical constants of a metal island film depend on the film composition and the island geometry (and thus also on the preparation method) in a rather complicated manner. As a practical consequence, thickness and effective optical constants of a metal island film can hardly be adjusted independently from each other.
- In metal island films, the effective refractive index may be comparable by magnitude to the effective extinction coefficient in broad spectral regions. This is in contrast to the behavior of familiar dielectric ($n \gg k$) or nearly ideally metallic ($n < k$) interference coating materials.
- Designs with metal island films will therefore necessarily show some absorption. Despite absorber specifications, this restricts the types of specifications where the use of metal island films makes sense to devices such as neutral density filters, asymmetric beamsplitters or decorative coatings and possibly color filters.
- The potential absorptance concept is an efficient tool for neutral density filter and beamsplitter design with metal island films.

Acknowledgements: The authors are grateful to Christopher Clark of Thin Film Center for many helpful discussions on optical coating design, and Norbert Kaiser for the invitation to write the tutorial and for his encouragement. The help of Josephine Wolf from Fraunhofer IOF in preparing several graphs is also gratefully acknowledged. Samples have been prepared by Hanno Heisse, Fraunhofer IOF, as well as Mario Held, Beschichtungstechnik Elsoff, Germany. Transmission electron microscopy investigations were performed by Johannes Biskupek und Ute Kaiser, Ulm University Germany.

Received June 26, 2012; accepted July 5, 2012

References

- [1] U. Kreibig and M. Vollmer, in 'Optical Properties of Metal Clusters' (Springer Series in Material Science 25, Springer-Verlag, Berlin, Heidelberg, New York, 1995).
- [2] D. G. Mie, *Ann. Phys.* 25, 377–445 (1908).
- [3] M. Born and E. Wolf, in 'Principles of Optics' (Pergamon Press, Oxford, 1968).
- [4] L. D. Landau and E. M. Lifschitz, in 'Lehrbuch der theoretischen Physik, Bd. VIII: Elektrodynamik der Kontinua [English translation: Textbook of Theoretical Physics, Vol. VIII: Electrodynamics of Continua]' (Akademie-Verlag, Berlin, 1985).
- [5] F. Stietz and F. Träger, *Physikalische Blätter* 55, 57 (1999).
- [6] A. Wokaun, *Solid State Phys.* 38, 223–294 (1984).
- [7] T. Yamaguchi, S. Yoshida and A. Kinbara, *Thin Solid Films* 21, 173–187 (1974).
- [8] J. M. Gerardy and M. Ausloos, *Phys. Rev. B* 25, 4204–4229 (1982).
- [9] M. Quinten, in 'Optical Properties of Nanoparticle Systems: Mie and Beyond' (Wiley VCH-Verlag&Co. KgaA, Weinheim, Germany, 2011).
- [10] A. N. Lebedev, M. Gartz, U. Kreibig and O. Stenzel, *Eur. Phys. J. D6*, 365–369 (1999).
- [11] A. N. Lebedev and O. Stenzel, *Eur. Phys. J. D7*, 83 (1999).
- [12] T. V. Amotchkina, V. Janicki, J. Sancho-Parramon, A. V. Tikhonravov, M. K. Trubetskov, et al., *Appl. Optics* 50, 1453–1464 (2011).
- [13] O. Stenzel, in 'The Physics of Thin Film Optical Spectra' (Springer-Verlag, Berlin, 2005).
- [14] K. H. Meiwes-Broer (Ed.), 'Metal Clusters at Surfaces (Springer Series in Cluster Physics)' (Springer Verlag, Berlin, 2000).
- [15] M. Held, O. Stenzel, S. Wilbrandt, N. Kaiser and A. Tünnermann, *Appl. Opt.* 51, 4436–4447 (2012).
- [16] P. Heger, O. Stenzel and N. Kaiser, *Proc. SPIE* 5250, 21 (2004).
- [17] T. V. Amotchkina, M. K. Trubetskov, A. V. Tikhonravov, V. Janicki, J. Sancho-Parramon, et al., *Appl. Optics* 50, 6189–6197 (2011).
- [18] O. Stenzel, S. Wilbrandt, A. Stendal, U. Beckers, K. Voigtsberger, et al., *J. Phys. D Appl. Phys.* 28, 2154 (1995).
- [19] P. H. Berning and A. F. Turner, *J. Optical Soc. Am.* 47, 230–239 (1957).
- [20] H. A. Macleod, *Thin-Film Optical Filters*, 4th edition (CRC Press, Boca Raton, FL, 2010).



Olaf Stenzel finished his diploma thesis in laser spectroscopy at the Physics Department of Moscow State University, Russia, in 1986. He received his PhD from Chemnitz University of Technology, Germany, in 1990 and habilitated there in 1999 in the field of optical properties of heterogeneous optical coatings. Since 2001, he has worked at the Optical Coating Department of Fraunhofer Institute for Applied Optics and Precision Engineering IOF in Jena, Germany. He is the author of 'The Physics of Thin Film Optical Spectra: An Introduction' (Springer, 2005).



Angus Macleod has more than 40 years of experience in optical coatings, both in manufacturing and in research. He was born and educated in Glasgow, Scotland, and worked both in industry and academia in the UK before joining the University of Arizona as Professor of Optical Sciences in 1979. Since 1995, he has been full-time with Thin Film Center, Inc., a software, training and consulting company in Tucson that he co-founded in 1986. He is the author of 'Thin Film Optical Filters', 4th edition (CRC Press, 2010).